Thermopower as a Sensitive Probe of Electronic Nematicity in Iron Pnictides

Shuai Jiang,[1,2] H. S. Jeevan,[1] Jinkui Dong,[1] and P. Gegenwart[1]
[1]I. Physikalisches Institut, Georg-August-Universität Göttingen, Göttingen, Germany
[2]1. Physikalisches Institut, Universität Stuttgart, Stuttgart, Germany
(Received 11 October 2012; published 4 February 2013)

We study the in-plane anisotropy of the thermoelectric power and electrical resistivity on detwinned single crystals of isovalent substituted $EuFe_2(As_{1-x}P_x)_2$. Compared to the resistivity anisotropy, the thermopower anisotropy is more pronounced and clearly visible already at temperatures much above the structural and magnetic phase transitions. Most remarkably, the thermopower anisotropy changes sign below the structural transition. This is associated with the interplay of two contributions due to anisotropic scattering and orbital polarization, which dominate at high and low temperatures, respectively.

DOI: 10.1103/PhysRevLett.110.067001 PACS numbers: 74.70.Xa, 74.25.fg, 74.40.Kb

Electronic states with broken rotational symmetry driven by electronic correlations rather than the anisotropy of the underlying crystal lattice have recently attracted considerable attention [1–5]. The iron-pnictide superconductors provide a new way to explore the relation of superconductivity (SC) and electronic nematicity. The AFe_2As_2, (A = Ba, Sr, Ca, or Eu) (“122”) materials crystallize in a tetragonal structure at high temperatures. Upon cooling through nearby structural (T_s) and magnetic (T_N) phase transitions, a low-temperature orthorhombic phase is stabilized where the Fe spins point along the (longer) a axis with antiferromagnetic (AFM) alignment [6]. Along the direction of the (shorter) b axis, neighboring spins are coupled ferromagnetically. The orthorhombic lattice distortion results in the formation of twin domains at $T < T_s$. A small uniaxial pressure along one of the orthorhombic in-plane directions is sufficient for detwinning [7].

Evidence for a pronounced in-plane electronic anisotropy of 122 systems below T_s has been found in the electrical resistivity [8], optical response to polarized light [9,10], quantum oscillations [11], and angular resolved photoemission spectroscopy (ARPES) [12]. The large energy separation of two orthogonal bands with predominant d_{xz} and d_{yz} character found in ARPES, sketched in the lower inset of Fig. 1, indicates an orbital polarization at low temperatures [12].

Remarkably, even for temperatures well above T_s, uniaxial stress induces a pronounced resistivity anisotropy [8]. Using a piezoelectric device, the resistivity anisotropy in the limit of *zero* strain has been detected [13]. Indeed, this “nematic susceptibility” diverges in the tetragonal state upon cooling from high T down to T_s, even once the latter is suppressed towards $T \to 0$ by doping. Importantly, electronic nematicity above T_s has also been confirmed on microcrystals with presumed unbalanced twin-domain volumes by magnetic torque measurements [14].

The origin of the resistivity anisotropy is controversially discussed. In one scenario, it is related to the orbital polarization, even at temperatures above T_s [15,16]. An alternative scenario has been proposed in [17]. The columnar AFM ground state of iron pnictides has a discrete Ising-type symmetry, related to stripes of parallel spins along one of the in-plane axes. Consequently, both the spin rotation and the Ising nematic symmetry are broken below T_N while the state at $T_N < T < T_s$ is characterized by the broken Ising-nematic symmetry only, with nematic spin fluctuations persisting above T_s [18]. As illustrated in the upper sketch of Fig. 1, the nonzero nematic susceptibility in the electrical resistivity is then caused by the anisotropic scattering of electrons near hot spots of the Fermi surface, connecting electron and hole pockets [in blue and red,

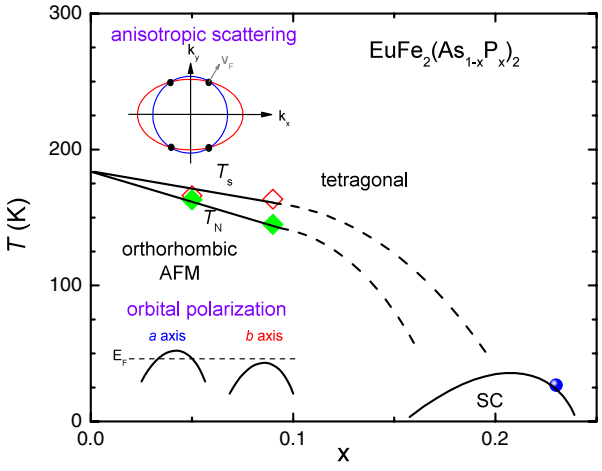

FIG. 1 (color online). Schematic phase diagram of $EuFe_2(As_{1-x}P_x)_2$, based on [19,20]. The ordering temperatures of Eu^{2+} magnetic moments have been omitted for clarity, as they are not important in the context of this study. Open diamond (red), solid diamond (green), and solid circle (blue) symbols denote structural (T_s), antiferromagnetic (T_N), and superconducting (SC) phase transitions shown in Figs. 2 and 5. The upper and lower cartoons illustrate the anisotropic scattering [18] and orbital polarization [12] scenario for the in-plane resistivity behavior, respectively. See text.

respectively, the latter (red) one has elliptical shape due to doping and is shifted by the critical wave vector $(\pi, 0)$].

Below, we establish the thermoelectric power (TEP) as a new and particularly sensitive probe of electronic nematicity in iron pnictides. Two distinct contributions from anisotropic scattering in the paramagnetic and orbital polarization in the AFM state are deduced. We focus on the isovalent substituted system $EuFe_2(As_{1-x}P_x)_2$, for which we have grown large and high-quality single crystals, which previously have been thoroughly characterized by bulk properties, ARPES, and optical conductivity [19–24]. The local Eu^{2+} magnetic moments order below about 20 K [25] and have negligible influence on the electronic properties of the system. Similarly as for $BaFe_2(As_{1-x}P_x)_2$, the partial substitution of As by isoelectronic smaller P induces a chemical pressure and suppresses the structural and spin-density-wave transitions found for undoped $EuFe_2As_2$ near 190 K. ARPES has revealed a nonrigid band change of the electronic structure with P substitution [21]. Roughly, the hole-Fermi surfaces become more three dimensional, thereby weakening the nesting conditions, whereas the size of the electron pocket near the K point slightly increases. The phase diagram is schematically depicted in the main part of Fig. 1. As a result of the presence of the Eu^{2+} local magnetic moments whose order below 20 K (not shown here) develops an increasing ferromagnetic component [22], bulk SC with $T_{c,\max}$ up to 26 K is found only in a narrow composition range and disappears beyond $x = 0.23$ [19,20] in contrast to previous reports on polycrystalline samples [26].

We investigate single crystals with compositions $x = 0.05$, 0.09, and 0.23 whose position in the phase diagram is indicated by the colored symbols in Fig. 1. Note that x denotes the composition determined by energy dispersive x-ray analysis (with uncertainty $\Delta x \approx 0.01$) rather than the nominal composition. The single crystals used in this study were synthesized and characterized as previously described [19]. After orientation, the single crystals were mounted in a uniaxial stress clamp for *in situ* detwinning at T_s. Details are provided in the Supplemental Material (SM) [27]. We used low-temperature polarized light imaging [28] in order to prove the single domain state below the structural phase transition. Following previous nomenclature, we use a and b for the longer and shorter in-plane orthorhombic axes, respectively. For TEP measurements, the heat flow between the sample and the clamp has been minimized by using thin plates of mica for thermal insulation [27]. The different samples have also been measured outside the clamp in suspended configuration. For a sample with negligible in-plane anisotropy ($x = 0.23$), we could use these measurements to determine a small temperature dependent background correction being proportional to the sample's surface attached to the pressure clamp, which has subsequently been subtracted from the raw data for $x = 0.05$ and $x = 0.09$ [27].

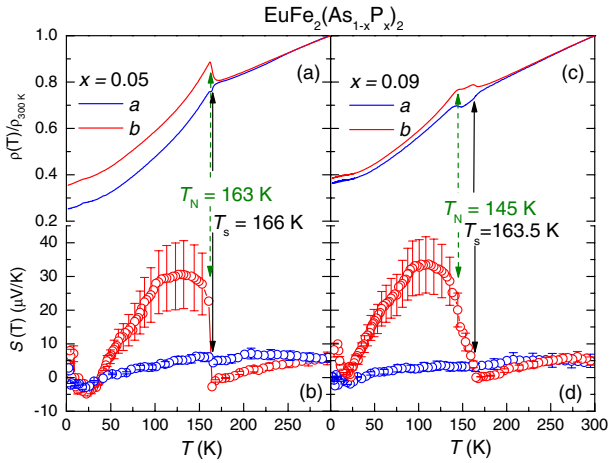

FIG. 2 (color online). Electrical resistivity (a) and (c) and thermoelectric power (b) and (d) of $EuFe_2(As_{1-x}P_x)_2$ along the orthorhombic a and b axes, indicated by blue and red, respectively. Solid arrows indicate structural phase transition (T_s) as determined by peak position of temperature derivative of resistivity anisotropy (see Fig. 3). The antiferromagnetic transition (T_N) is obtained from the (lower) kink of the resistivity data along the b axis and denoted by the dashed arrows.

We first focus on results on two "underdoped" $x = 0.05$ and $x = 0.09$ samples, and discuss their resistivity anisotropy above and below the structural and magnetic transitions. As shown in Figs. 2(a) and 2(c), the electrical resistivity along the a and b axes (ρ_a and ρ_b) displays an almost linear temperature dependence upon cooling from room temperature. However, a careful inspection of the relative difference $\Delta\rho = \frac{\rho_b - \rho_a}{\rho_b + \rho_a}$ reveals an anisotropy in the percentage range already in this temperature regime (see Fig. 3). We use the sharp peak in the temperature derivative $d\Delta\rho/dT$ to define the position of T_s, since at this temperature, the maximal increase of anisotropy is found. As shown in the SM (inset of Fig. S3), we also find clear peaks in the temperature derivatives of $\rho_a(T)$ and $\rho_b(T)$ at the same temperature. The AFM transition occurs at slightly lower temperatures and gives rise to a further anomaly in the resistivity, which is most prominent along the b axis. Note that the separation between T_s and T_N increases with increasing x [20]. At low temperatures, the resistivity along the b axis is distinctly higher than that along the a axis, similar to that found in "electron-doped" $Ba(Fe_{1-x}Co_x)_2As_2$ [8] and $Eu(Fe_{1-x}Co_x)_2As_2$ [29].

We now turn to the respective anisotropy found in the TEP shown in Figs. 2(b) and 2(d). As indicated by the solid (T_s) and dashed (T_N) lines, sharp and well-defined signatures, in particular for the data along the b axis, are resolved at the phase transitions. The signature along a is small but clearly visible also in the raw data [27]. At high temperature, $S_b(T)$ decreases with decreasing T. At T_s, a sharp increase of S_b is found along with a further change in slope at T_N, which is most prominently seen for the $x = 0.09$ sample. After passing a maximum around 100 K,

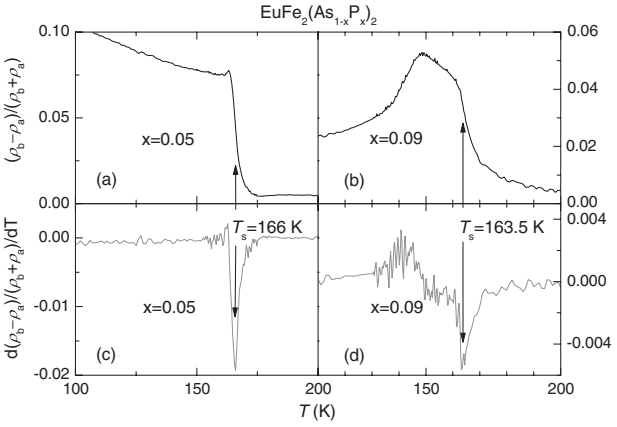

FIG. 3. Temperature dependence of the normalized electrical resistivity anisotropy $(\rho_b - \rho_a)/(\rho_b + \rho_a)$ for $EuFe_2(As_{0.95}P_{0.05})_2$ (a) and $EuFe_2(As_{0.91}P_{0.09})_2$ (b), as well as respective temperature derivatives (c) and (d). Solid arrows indicate T_s as determined from minima in (c) and (d).

$S_b(T)$ then decreases and displays a broadened minimum near 25 K. We have found similar overall behavior in our previous investigation on twinned single crystals of similar compositions [24], indicating a dominating contribution from S_b in this latter case. The low-temperature minimum near 25 K has also been found for the hole-doped system $Eu_{1-x}K_xFe_2As_2$ and has been ascribed to a negative phonon drag contribution [24].

In order to discuss the anisotropy of the TEP, we calculate the difference $\Delta S(T) = S_b(T) - S_a(T)$ between the data along the b and a axes and analyze its temperature dependence (for a plot of the normalized difference, see the SM [27]). As shown in Fig. 4, $\Delta S(T)$ changes sign at T_s: while it is negative at high temperature, a sharp rise sets in at T_s, resulting in positive values at least below T_N. This is our most important observation and indicates a distinct difference from the electrical resistivity anisotropy, which does not change sign. Furthermore, the normalized anisotropy of the TEP [27] is far more pronounced than that of the electrical resistivity, demonstrating the great sensitivity of this property to electronic nematicity.

Generally, the TEP contains a "drift" contribution from the charge separation due to a thermal gradient and a "drag" contribution originating from the lattice polarization by the charge carriers. Since the latter contribution typically dominates only at low temperatures $\sim\Theta_D/5$, we relate the observed anisotropy of the TEP to the anisotropy of the drift contribution. Using the Boltzmann equation within the relaxation-time ansatz in the Sommerfeld approximation for a degenerate Fermi gas, the drift TEP is given by the Mott formula

$$S = \frac{\pi^2 k_B^2 T}{3e} \frac{\partial \ln\sigma(E)}{\partial E}\bigg|_{E_F}, \qquad (1)$$

which relates the TEP to the logarithmic energy derivative of the electrical (dc) conductivity σ at the Fermi energy.

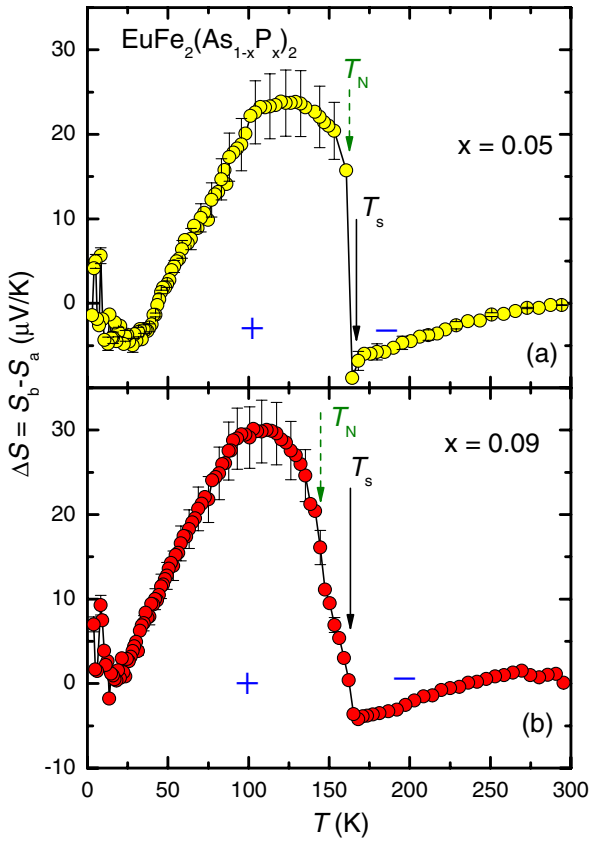

FIG. 4 (color online). Temperature dependence of the TEP anisotropy $\Delta S = S_b(T) - S_a(T)$ for $EuFe_2(As_{0.95}P_{0.05})_2$ (a) and $EuFe_2(As_{0.91}P_{0.09})_2$ (b). Solid and dashed arrows indicate T_s and T_N, respectively, as determined from the electrical resistivity (cf. Fig. 1 and resistivity anisotropy, Fig. 3). Plus (+) and minus (−) symbols indicate sign of thermopower anisotropy.

Assuming a simple relation $\sigma \propto lS_F$, where l denotes the mean-free path and S_F the Fermi surface area, reveals

$$S = \frac{\pi^2 k_B^2 T}{3e}\left(\frac{\partial \ln l}{\partial E}\bigg|_{E_F} + \frac{\partial \ln S_F}{\partial E}\bigg|_{E_F}\right). \qquad (2)$$

The two contributions to the TEP are arising from the scattering, determining the mean-free path, and from the band structure. The in-plane anisotropy of the TEP under a small uniaxial pressure is therefore determined by the sum of the terms reflecting the anisotropies of the mean-free path and Fermi surface, respectively. The former will be affected by anisotropic scattering due to magnetic fluctuations while the latter is induced by orbital polarization. The Fermi surface reconstruction below T_N may also add to the latter contribution. However, mean-field calculations have revealed that the observed band anisotropy could not be explained by magnetic order alone and requires orbital polarization [30]. Given that the TEP anisotropy depends on the anisotropy of l and S_F, the question arises which term dominates in which temperature regime.

At temperatures above T_s, the orbital polarization is weak and, respectively, the strain dependence of the Fermi surface is expected to be small. On the other hand, nematic spin fluctuations will result in a pronounced anisotropy of the mean-free path. Since the resistivity along the (shorter) b direction is higher than along a, the uniaxial pressure dependence of the mean-free path is negative along b and positive along a, leading to $\Delta S = S_b - S_a < 0$. This contribution is expected to decrease below T_N once the spin fluctuations are suppressed.

The dramatic increase of $\Delta S(T)$ at $T \leq T_s$ likely reflects the dominance of the orbital polarization, leading to a significant shift of the density of states below the Fermi energy along the b axis (cf. lower sketch in Fig. 1). Respectively, a large increase of the TEP is found along this direction, resulting in $\Delta S > 0$.

Within this picture the sign change of TEP points to the competition of two contributions due to anisotropic fluctuations, dominating at high temperatures, and orbital polarization, dominating at low temperatures. If, as proposed in [15], the orbital polarization would be dominating already at high temperatures and be the driver of the anisotropy in the initial strain dependence of the resistivity, a sign change of TEP would not arise. Therefore, our data support the view [18] that nematicity at high temperatures results from anisotropic magnetic scattering.

At last, we focus on a composition $x = 0.23$ in the slightly "overdoped" regime of the phase diagram of $EuFe_2(As_{1-x}P_x)_2$ (cf. Fig. 1). A previous ARPES study on the system has revealed a Lifshitz transition near $x = 0.21$ at which the inner hole pocket along Γ-Z disappears [21]. The thermopower $S(x)$, being very sensitive to the Fermi surface, has detected a nonmonotonic evolution at this concentration at all investigated temperatures [24], similar to that found near Lifshitz transitions in electron-doped $Ba(Fe_{1-x}Co_x)_2As_2$ [31]. The structural transition is completely suppressed for $x = 0.23$ in accordance with the phase diagram. Indeed, as shown in Fig. 5(a), almost no in-plane anisotropy of the electrical resistivity could be detected. No reliable anisotropy of the TEP could be detected either [27] and the data agree within the experimental error with those measured previously without uniaxial pressure clamp [24]. Therefore, Fig. 5(b) only includes data measured without uniaxial pressure.

Similar to that found for the related system $BaFe_2(As_{1-x}P_x)_2$ [32], an almost linear temperature dependence of the normal-state electrical resistivity is found from T_c up to room temperature [cf. dotted line in Fig. 5(a)]. This non-Fermi liquid behavior is further corroborated by the logarithmically divergent coefficient of the TEP, $S/T \propto \log T$ shown in Fig. 5(b). These temperature dependences would be compatible with two-dimensional AFM quantum critical fluctuations [33]. The same conclusion has also been drawn from NMR measurements on $BaFe_2(As_{1-x}P_x)_2$ [34], and a sharp peak of the

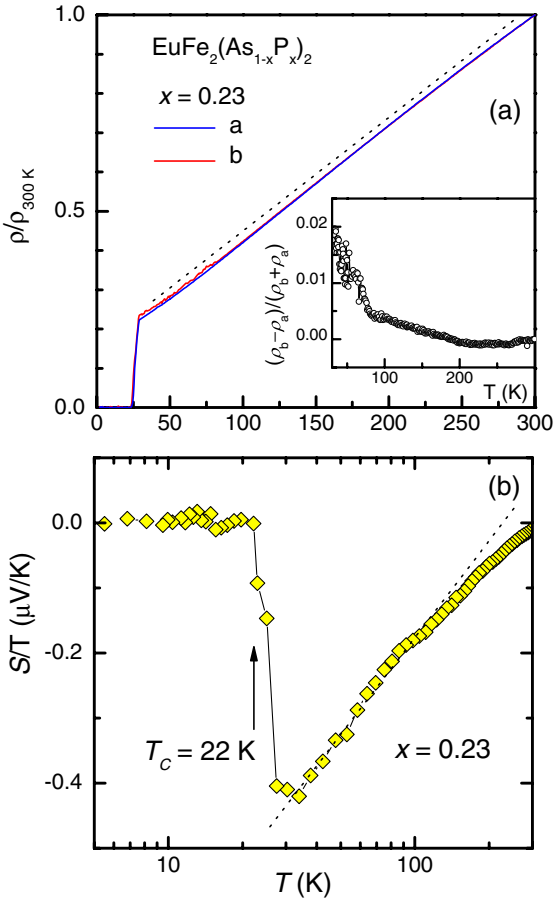

FIG. 5 (color online). Temperature dependence of the electrical resistivity (a) and TEP (b) for $EuFe_2(As_{0.77}P_{0.23})_2$ [(a) and (b) denote in-plane tetragonal (110) directions perpendicular and parallel to the applied uniaxial pressure, which in the orthorhombic notation would correspond to the respective main axes; however, there is no orthorhombic phase in this sample]. For (b) data along the tetragonal (110) axis without uniaxial pressure are shown [27]. The inset in (a) displays the resistivity anisotropy in the normal state. Dashed lines are intended as guides to the eye and the arrow indicates transition into the SC state.

zero-temperature SC penetration depth for this latter system suggests a quantum critical point located in the SC state at optimum substitution [35].

We have used the TEP to investigate electronic nematicity in the isovalent substituted iron pnictide $EuFe_2(As_{1-x}P_x)_2$ on detwinned single crystals using a uniaxial-pressure technique. It turns out that TEP is a very sensitive probe and displays a pronounced anisotropy for low substitution x. Remarkably, this anisotropy changes sign upon cooling from above to below the structural phase transition. We propose two contributions of opposite sign arising from anisotropic scattering dominating at $T > T_s$ and orbital polarization for $T < T_s$. For the future, it will be interesting to perform similar experiments on hole-doped 122 pnictides, for which previous electrical resistivity measurements have found an opposite sign of

the anisotropy [36]. Our results should also motivate theoretical work on the influence of spin fluctuations to the TEP anisotropy.

We thank R. M. Fernandes, I. R. Fisher, W. Ku, J. Schmalian, and Z. W. Zhu for informative discussions, J. Maiwald for help with the TTO option of the PPMS, and J. Norpoth and C. Jooss for providing access to a low-temperature polarized light microscope. S. J. and J. D. acknowledge support from the Alexander von Humboldt Foundation. This work is supported by the DFG through SPP 1458.

[1] S. A. Kivelson, E. Fradkin, and V. J. Emery, Nature (London) **393**, 550 (1998).
[2] R. A. Borzi, S. A. Grigera, J. Farrell, R. S. Perry, S. J. S. Lister, S. L. Lee, D. A. Tennant, Y. Maeno, and A. P. Mackenzie, Science **315**, 214 (2007).
[3] R. Daou *et al.*, Nature (London) **463**, 519 (2010).
[4] R. Okazaki, T. Shibauchi, H. J. Shi, Y. Haga, T. D. Matsuda, E. Yamamoto, Y. Onuki, H. Ikeda, and Y. Matsuda, Science **331**, 439 (2011).
[5] C. Stingl, R. S. Perry, Y. Maeno, and P. Gegenwart, Phys. Rev. Lett. **107**, 026404 (2011).
[6] Q. Huang, Y. Qiu, W. Bao, M. A. Green, J. W. Lynn, Y. C. Gasparovic, T. Wu, G. Wu, and X. H. Chen, Phys. Rev. Lett. **101**, 257003 (2008).
[7] I. R. Fisher, L. Degiorgi, and Z. X. Shen, Rep. Prog. Phys. **74**, 124506 (2011).
[8] J.-H. Chu, J. G. Analytis, K. De Greve, P. L. McMahon, Z. Islam, Y. Yamamoto, and I. R. Fisher, Science **329**, 824 (2010).
[9] A. Dusza, A. Lucarelli, F. Pfuner, J.-H. Chu, I. R. Fisher, and L. Degiorgi, Europhys. Lett. **93**, 37 002 (2011).
[10] M. Nakajima *et al.*, Proc. Natl. Acad. Sci. U.S.A. **108**, 12 238 (2011).
[11] T. Terashima *et al.*, Phys. Rev. Lett. **107**, 176402 (2011).
[12] M. Yi *et al.*, Proc. Natl. Acad. Sci. U.S.A. **108**, 6878 (2011).
[13] J. H. Chu, H.-H. Kuo, J. G. Analytis, and I. R. Fisher, Science **337**, 710 (2012).
[14] S. Kasahara *et al.*, Nature (London) **486**, 382 (2012).
[15] C.-C. Chen, J. Maciejko, A. P. Sorini, B. Moritz, R. R. P. Singh, and T. P. Devereaux, Phys. Rev. B **82**, 100504 (2010).
[16] B. Valenzuela, E. Bascones, and M. J. Calderon, Phys. Rev. Lett. **105**, 207202 (2010).
[17] R. M. Fernandes, E. Abrahams, and J. Schmalian, Phys. Rev. Lett. **107**, 217002 (2011).
[18] R. M. Fernandes and J. Schmalian, Supercond. Sci. Technol. **25**, 084005 (2012).
[19] H. S. Jeevan, D. Kasinathan, H. Rosner, and P. Gegenwart, Phys. Rev. B **83**, 054511 (2011).
[20] Y. Tokiwa, S.-H. Hübner, O. Beck, H. S. Jeevan, and P. Gegenwart, Phys. Rev. B **86**, 220505(R) (2012).
[21] S. Thirupathaiah *et al.*, Phys. Rev. B **84**, 014531 (2011).
[22] S. Zapf, D. Wu, L. Bogani, H. S. Jeevan, P. Gegenwart, and M. Dressel, Phys. Rev. B **84**, 140503 (2011).
[23] D. Wu, G. Chanda, H. S. Jeevan, P. Gegenwart, and M. Dressel, Phys. Rev. B **83**, 100503 (2011).
[24] J. Maiwald, H. S. Jeevan, and P. Gegenwart, Phys. Rev. B **85**, 024511 (2012).
[25] Y. Xiao *et al.*, Phys. Rev. B **80**, 174424 (2009).
[26] Z. Ren, Q. Tao, S. Jiang, C. Feng, C. Wang, J. Dai, G. Cao, and Z. Xu, Phys. Rev. Lett. **102**, 137002 (2009).
[27] See Supplemental Material at http://link.aps.org/supplemental/10.1103/PhysRevLett.110.067001 for details on sample preparation, the experimental setup, the electrical resistivity, and thermoelectric power measurements.
[28] M. A. Tanatar, A. Kreyssig, S. Nandi, N. Ni, S. L. Bud'ko, P. C. Canfield, A. I. Goldman, and R. Prozorov, Phys. Rev. B **79**, 180508(R) (2009).
[29] J. J. Ying *et al.*, Phys. Rev. Lett. **107**, 067001 (2011).
[30] Weicheng Lv and Philip Phillips, Phys. Rev. B **84**, 174512 (2011).
[31] C. Liu *et al.*, Phys. Rev. B **84**, 020509 (2011).
[32] S. Kasahara *et al.*, Phys. Rev. B **81**, 184519 (2010).
[33] I. Paul and G. Kotliar, Phys. Rev. B **64**, 184414 (2001).
[34] Y. Nakai, T. Iye, S. Kitagawa, K. Ishida, H. Ikeda, S. Kasahara, H. Shishido, T. Shibauchi, Y. Matsuda, and T. Terashima, Phys. Rev. Lett. **105**, 107003 (2010).
[35] K. Hashimoto *et al.*, Science **336**, 1554 (2012).
[36] E. C. Blomberg, M. A. Tanatar, R. M. Fernandes, B. Shen, H.-H. Wen, J. Schmalian, and R. Prozorov, arXiv:1202.4430.